

State-to-state dynamics of reactions H+DH'(v 0, j =0) → HH'(v',j')+D/HD(v',j')+H' with time-dependent quantum wave packet method

Juan Zhao(赵娟), Da-Guang Yue(岳大光), Lu-Lu Zhang(张路路), Shang Gao(高尚), Zhong-Bo Liu(刘中波), and Qing-Tian Meng(孟庆田)

Citation: Chin. Phys. B, 2021, 30 (**7**): 073102. DOI: 10.1088/1674-1056/abf559
Journal homepage: http://cpb.iphy.ac.cn; http://iopscience.iop.org/cpb

What follows is a list of articles you may be interested in

Mechanism analysis of reaction $S^+(^2D)+H_2(X^1\Sigma_g^+)\rightarrow SH^+(X^3\Sigma^-)+H(^2S)$ based on the quantum state-to-state dynamics

Jin-Yu Zhang(张金玉), Ting Xu(许婷), Zhi-Wei Ge(葛志伟), Juan Zhao(赵娟), Shou-Bao Gao(高守宝), Qing-Tian Meng(孟庆田)

Chin. Phys. B, 2020, 29 (**6**): 063101. DOI: 10.1088/1674-1056/ab889c

Effect of isotope on state-to-state dynamics for reactive collision reactions $O(^3P)+H_2^+\rightarrow OH^++H$ and $O(^3P)+H_2^+\rightarrow OH+H^+$ in ground state $1^2A''$ and first excited $1^2A'$ potential energy surfaces

Juan Zhao(赵娟), Ting Xu(许婷), Lu-Lu Zhang(张路路), Li-Fei Wang(王立飞)

Chin. Phys. B, 2020, 29 (**2**): 023105. DOI: 10.1088/1674-1056/ab6554

Dynamics of the Au+H_2 reaction by time-dependent wave packet and quasi-classical trajectory methods

Yong Zhang(张勇), Chengguo Jiang(姜成果)

Chin. Phys. B, 2019, 28 (**12**): 123101. DOI: 10.1088/1674-1056/ab52f2

Reaction mechanism of D+ND→N+D_2 and its state-to-state quantum dynamics

Ting Xu(许婷), Juan Zhao(赵娟), Xian-Long Wang(王宪龙), Qing-Tian Meng(孟庆田)

Chin. Phys. B, 2019, 28 (**2**): 023102. DOI: 10.1088/1674-1056/28/2/023102

State-to-state dynamics of $F(^2P)+HO(^2\Pi)\rightarrow O(^3P)+HF(^1\Sigma^+)$ reaction on $1^3A''$ potential energy surface

Juan Zhao(赵娟), Hui Wu(吴慧), Hai-Bo Sun(孙海波), Li-Fei Wang(王立飞)

Chin. Phys. B, 2018, 27 (**2**): 023102. DOI: 10.1088/1674-1056/27/2/023102

State-to-state dynamics of reactions $H + DH'(v = 0, j = 0) \rightarrow HH'(v', j') + D/HD(v', j') + H'$ with time-dependent quantum wave packet method*

Juan Zhao(赵娟)[1], Da-Guang Yue (岳大光)[1], Lu-Lu Zhang(张路路)[1], Shang Gao(高尚)[1], Zhong-Bo Liu(刘中波)[1], and Qing-Tian Meng(孟庆田)[2,†]

[1] *School of Science, Shandong Jiaotong University, Jinan* 250357, *China*
[2] *School of Physics and Electronics, Shandong Normal University, Jinan* 250358, *China*

(Received 12 March 2021; revised manuscript received 1 April 2021; accepted manuscript online 7 April 2021)

State-to-state time-dependent quantum dynamics calculations have been carried out to study $H + DH' \rightarrow HH' + D/HD + H'$ reactions on BKMP2 surface. The total integral cross sections of both reactions are in good agreement with earlier theoretical and experimental results, moreover the rotational state-resolved reaction cross sections of $H + DH' \rightarrow HH' + D$ at collision energy $E_C = 0.5$ eV are closer to the experimental values than the ones calculated by Chao *et al.* [*J. Chem. Phys.* **117** 8341 (2002)], which proves the higher precision of the quantum calculation in this work. In addition, the state-to-state dynamics of $H + DH' \rightarrow HD' + H$ reaction channel have been discussed in detail, and the differences of the micro-mechanism of the two reaction channels have been revealed and analyzed clearly.

Keywords: state-to-state, time-dependent quantum wave-packet method, differential cross sections

PACS: 31.15.xv, 34.50.−s, 03.67.Lx **DOI:** 10.1088/1674-1056/abf559

1. Introduction

The $H + H_2$ reaction and its isotopic variants have been the focus of numerous experimental[1–7] and theoretical[8–17] studies over many years. In the field of molecular reaction dynamics, the construction of potential energy surface (PES) is very important. For $H + H_2$ system, there are a lot of works about PES. As early as in 1978, Truhlar *et al.* have developed LSTH surface[18] with 267 *ab initio* points and a maximum absolute deviation of 0.55 kcal/mol. In 1987, Varandas *et al.* performed complete-active-space self-consistent field (CASSCF) and multireference configuration interaction calculation and gave an adiabatic double many-body expansion (DMBE) PES for H_3.[19] In 1994, Sun *et al.* carried out quantum mechanical calculations of the rotational excitation of H_2 by H atoms using the DMBE[19] PES and found that the low temperature thermal rate coefficients were significantly higher than those based on the LSTH[18] surface. In order to investigate the origin of these discrepancies between these two H_3 PESs, Boothroyd *et al.* developed an improved surface (BKMP),[20] which matched the 772 *ab initio* energies with a maximum absolute deviation of 1.21 kcal/mol. BKMP surface incorporated new data extending to $R_{H-H_2} = 4a_0$, but it too was least well constrained in the critical range of R_{H-H_2}. In 1996, Boothroyd *et al.* fitted a refined H_3 PES, denoted as BKMP2[21] surface, this PES was based on 8701 *ab initio* energies with an overall root-mean-square (rms) error of 0.17 kcal/mol and a maximum absolute deviation of 3.90 kcal/mol. In 1999, Wu *et al.*[22] calculated a new surface based on spline fits of an exact quantum Monte Carlo method.

Based on these five surfaces, numerous theoretical studies of the H_3 system have been done, among which the BKMP2 surface is most widely used[23–27] for the reason that in accurate quantum calculation, it can produce a very good agreement result with the experiment.[2,3,28–31] In 1997, Hochman–Kowal and Persky[32] studied the influence of rotation on reactivity for the $H + DH(v = 0, j = 0–6)$ on the LSTH and DMBE PESs using the quasi-classical trajectory method. In 2002, Chao *et al.*[3,28] presented the results of a joint experimental and theoretical investigation of the reaction dynamics of the $H + DH' \rightarrow D + HH'$ chemical reaction, and found that the experimental and theoretical state-to-state dynamics are in quantitative agreement.

The above researches mainly focus on $H + DH' \rightarrow D + HH'$ channel, but the collisions between H and DH may generate products through two reaction channels: the abstraction channel that produces the production of H_2 ($H + DH' \rightarrow HH' + D$) and the exchange channel that leads to the production of HD ($H + DH' \rightarrow HD' + H$), the study of exchange channel $H + DH' \rightarrow HD' + H$ is few. In addition, Han *et al.*[33] developed a parallel code for state-to-state quantum dynamics with propagation of time-dependent wave-packet[34,35] (TDWP) in reactant coordinates based on graphical processing

*Project supported by the National Natural Science Foundation of China (Grant Nos. 11504206 and 12004216), the Ph. D. Research Start-up Fund of Shandong Jiaotong University (Grant No. BS2020025), and the Shandong Natural Science Foundation, China (Grant Nos. ZR2020MF102 and ZR2020QA064).

†Corresponding author. E-mail: qtmeng@sdnu.edu.cn

© 2021 Chinese Physical Society and IOP Publishing Ltd

units (GPUs), and this code has been used to calculate the differential cross sections (DCSs) of $H+H_2$ reaction based on the BKMP2 surface and state-resolved reaction probabilities of nonadiabatic triplet–singlet transitions of $O(^3P,^1D)+H_2$[33] for the total angular momentum $J=0$. These results show that the calculation accuracy is high and the calculation speed is fast, which solves the time-consuming and memory limitation problems that have troubled researchers for a long time due to the large amount of state-to-state quantum calculation. So far, this code has been successfully used to study the quantum state-to-state dynamics of $O(^3P)+HD$,[36] $S+H_2$,[37] $N+H_2$,[38] $N+HD$,[39] $F+HO$,[40] $D+ND$[41] reactions.

In this work, we used this efficient GPUs version of time-dependent wavepacket code to calculate the product state-resolved integral cross sections (ICSs) and differential cross sections of $H+DH'\rightarrow HH+D'$ and $H+DH'\rightarrow HD+H'$ reaction channels. The paper is organized as follows: in Section 2, we will give the theoretical methodology used in this work. Section 3 will present the results and discussion. Finally Section 4 will close with the conclusions.

2. Theoretical method

In this contribution, the efficient GPUs version of TDWP[33] code is used. This code has been successfully applied to many studies on the state-to-state dynamics properties of $A+BC$ system.[36–43] The main idea of this method is as follows. The Hamiltonian of the title reaction is defined in the body-fixed (BF) reactant Jacobi coordinates. For a given J (J is total rotational angular momentum), the Hamiltonian of the $A+BC$ reaction can be expressed as

$$H=-\frac{\hbar^2}{2\mu_R}\frac{\partial^2}{\partial R^2}+\frac{(\hat{J}-\hat{j})^2}{2\mu_R R^2}+\frac{\hat{j}^2}{2\mu_r r^2}+h(r)+V(R,r,\theta), \quad (1)$$

The corresponding reduced mass μ_R is expressed as $\mu_R=m_A\cdot(m_B+m_C)/(m_A+m_B+m_C)$, and μ_r can be written as $\mu_r=m_B\cdot m_C/(m_B+m_C)$. $\hat{J}$ is the total angular momentum operator, and $\hat{j}$ is the rotational angular momentum operator of BC. $V(R,r,\theta)=V_{pes}-V_r(r)$, where V_{pes} is the potential energy of the triatomic system, and $V_r(r)$ is the diatomic potential energy of BC. $h(r)$ is the diatomic reference Hamiltonian defined as

$$h(r)=-\frac{\hbar^2}{2\mu_r}\frac{\partial^2}{\partial r^2}+V_r(r). \quad (2)$$

The initial Gaussian wave packet for the reactant in the space-fixed (SF) reactant Jacobi coordinate is expanded as:

$$|\chi_i\rangle=\varphi^{JM\varepsilon}_{\alpha v_0 j_0 l_0}=G(R_\alpha)\phi_{v_0 j_0}(r_\alpha)\,|JMj_0l_0\varepsilon\rangle\,. \quad (3)$$

For the initial state $(v_0j_0l_0)$, $|JMj_0l_0\varepsilon\rangle$ represents the SF rotational basis and describes angular motion, with M being the projection of the total angular momentum J . $\phi_{v_0j_0}(r_\alpha)$ is the rovibrational eigen-function of the diatomic molecule BC. The initial wave packet is transformed into the BF frame and propagated on GPUs with the second-order split method.[44] The absorbing potentials with the form of damping functions are employed to prevent the reflections of the wave packet from the boundaries. To extract the state-to-state information of the product channels, the handicap of the reactant Jacobi coordinate based method is the coordinate transformation from reactant to product channel, and the radial component of product wave-packet is a delta function multiplied the outgoing asymptotic radial functions

$$|\chi_f\rangle=\delta(R-R_\infty)\phi_{v_f j_f}(r_\beta)\,|JMj_fl_f\rangle\,, \quad (4)$$

where R_∞ is the location of the dividing surface in the product asymptote where the transformation proceeds. The basic idea of the transformation is to carry out the projection from the wave packet in the reactant Jacobi coordinate $(R_\infty,r_\alpha,\theta_\alpha,K_\alpha)$ to the product Jacobi coordinate $(R_\infty,r_i,\theta_j,K_\beta)$ through the equation, with K_α and K_β being the projection of the total angular momentum J in the BF reactant and product coordinates, respectively. So, the scattering matrix element in BF representation is defined as

$$S_{if}(E)=\frac{1}{2\pi a_{\alpha i}(E)a^*_{\beta f}(E)}\int_{-\infty}^{+\infty}dt e^{(i/\hbar)Et}\langle\chi_{\beta f}|e^{(i/\hbar)\hat{H}t}|\chi_{\alpha i}\rangle\,. \quad (5)$$

The coefficients are given by

$$\begin{aligned}a_{\alpha i}(E)&=\left\langle\phi_i\left|\chi_i^+\right.\right\rangle\\&=\left\langle i\sqrt{\frac{\mu_R k_{\alpha i}}{2\pi}}Rh^{(2)}_{l_{\alpha i}}(k_{\alpha i}R)\middle|G(R_\alpha)\right\rangle, \quad (6)\\ a_{\beta f}(E)&=\left\langle\phi_f\left|\chi_f^+\right.\right\rangle\\&=\left\langle\sqrt{\frac{\mu_R k_{\beta f}}{2\pi}}Rh^{(1)}_{l_{\beta f}}(k_{\beta f}R)\middle|\delta(R-R_\infty)\right\rangle, \quad (7)\end{aligned}$$

where $h^{(1,2)}$ are the spherical Hankel functions of the first and second kinds. Finally, the scattering matrix is transformed into helicity representation to derive the DCS and ICS by a scattering matrix summing over all relevant total angular momentum quantum numbers J.

$$\begin{aligned}\frac{d\sigma_{v'j',v_0j_0}(\theta,E)}{d\Omega}&=\frac{1}{(2j_0+1)}\sum_{K'}\sum_{K_0}\left|\frac{1}{2ik_{v_0j_0}}\sum_J(2J+1)\right.\\&\left.\times d^J_{K'K_0}(\theta)S^J_{v'j'K',v_0j_0K_0}\right|^2, \quad (8)\\ \sigma_{v'j',v_0j_0}&=\frac{1}{(2j_0+1)k^2_{v_0j_0}}\\&\times\sum_{K'}\sum_{K_0}\sum_J(2J+1)\left|S_{v'j'K',v_0j_0K_0}\right|^2, \quad (9)\end{aligned}$$

where $k_{v_0j_0}$ is the translational wave vector of the initial state (v_0,j_0). θ is the scattering angle and $d^J_{K'K_0}$ is the Wigner

rotational matrix. More theoretical details can be found in Ref. [33].

In present work, we carry out state-to-state calculation for all angular momentum J up to 30 to converge differential cross sections of the title reaction for the collision energy range of 0.15 eV–1.0 eV. To insure convergence of scattering results, extensive tests have been carried out to determine the optimal parameters, which are summarized in Table 1. One of the key convergence parameters in this work is denoted K, which is set $(J+1)$, including all the projection of the total angular momentum J.

Table 1. Numerical parameters used in the present quantum wave packet calculations.

Parameter	Value
Product Jacobi coordinate (R) range	0.002 a_0–16.0 a_0
No. grid points in R	120
No. translational basis functions in the interaction region	50
Product Jacobi coordinate (r) range	0.5 a_0–11.2 a_0
No. grid points in r	500
No. vibrational basis functions in the interaction region	300
No. angular grid points	50
Center of initial wave packet (R_0)	8.0 a_0
Width of the wave packet (δ)	0.7 a_0
Integration time interval (Δ)	5 a.u.
Absorption length in R and r	4.0/4.0 a_0
Absorption strength in R and r	0.12/0.12
Propagation time	10 000 a.u.

3. Results and discussion

3.1. Reaction probability and integral cross section

Figure 1 shows the minimum energy path (MEP) of H3 BKMP2 PES. As is shown in Fig. 1, there is a barrier with the height of 9.61 kcal/mol ($\approx$ 0.42 eV).[21]

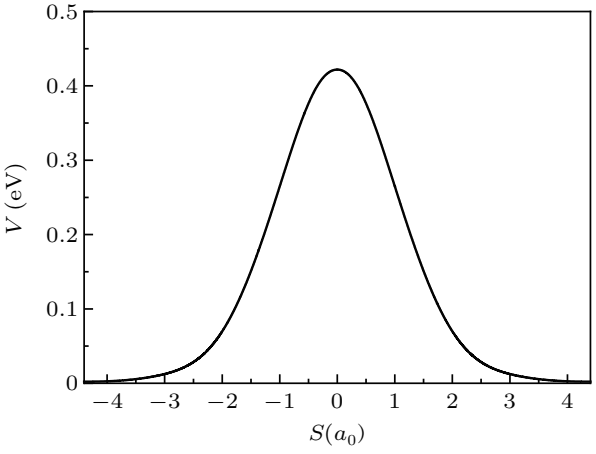


Fig. 1. Minimum energy path of the BKMP2 PES.

Firstly, in order to verify the correctness of our calculations, the ICSs summed over final states of $H + DH' \rightarrow HH' + D$ and $HD + H'$ reaction channels and the rotational state-resolved ICS of $H + DH' \rightarrow HH' + D$ at the collision energy of 0.5 eV are calculated, and the results are shown in Figs. 2(a) and 2(b), respectively. In Fig. 2(a), the green dash-dot line are TDWP results of $H + DH' \rightarrow HH' + D$, the blue dash-dot-dot line are TDWP results of $H + DH' \rightarrow HD + H'$ channel in this work, and the other results are cited from Refs. [28,32]. As shown in Fig. 2(a), all the ICSs present a similar trend, *i.e.*, each of them increases with increasing relative translational energy and has a threshold at energy of about 0.35 eV. Due to the quantum tunneling effect, the threshold energy is smaller than the height of barrier. There are also differences between the two reaction channels in Fig. 2(a). The reaction section value of the $HD + H'$ channel is larger than that of the $HH' + D$ channel at the collision energy higher than 0.5 eV. There are two possible reasons; one is the zero-point energy (ZPE) effect, the other is the deviation of the center of mass of the reactant molecule DH'. For $H + DH'$ reaction system, the force constant of the reaction system is the same, but the vibrational frequency of HD substitute is lower than HH', so the harmonic ZPE of the HD molecule is lower than HH', the $H + DH' \rightarrow HD + H'$ is easier to occur, and the cross section is larger. Moreover, from a classical point of view, the center of mass of the reactant molecule DH' is closer to the D atom, so when H atoms collides with DH' molecule, the probability of H atoms hitting D will be greatly increased, resulting in the formation

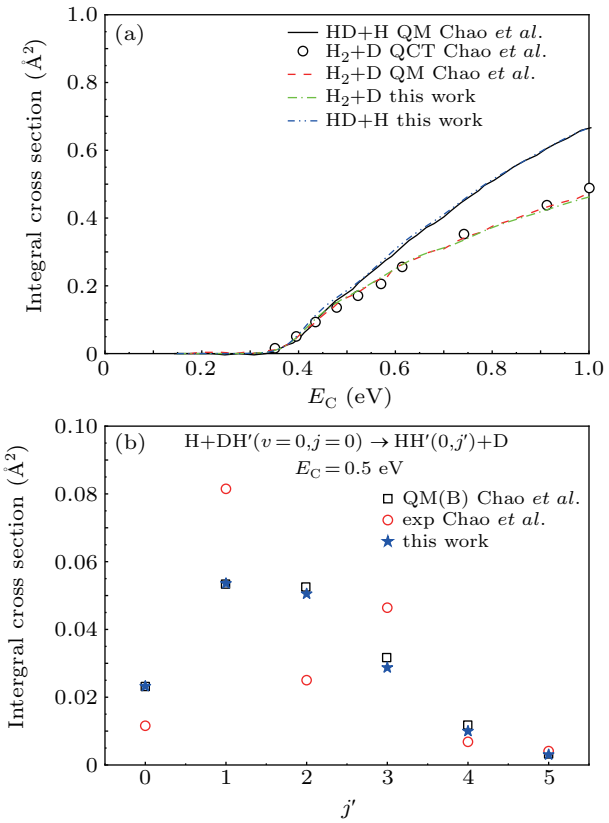


Fig. 2. (a) Total ICSs *versus* collision energy. The early QM results are from Chao and Skodje (Ref. [28]), the QCT results are from Hochman–Kowal and Persky (Ref. [32]). (b) The ICS for $H + DH'(v = 0, j = 0) \rightarrow HD(v' = 0, j') + H'$ *versus* j' at $E_C = 0.5$ eV. The red circles are the experimental results (Ref. [28]) and black squares represent the results of QM using Boltzmann statistics (Ref. [28]).

of HD products more easily, and the integral cross section of HD + H′ is larger than that of the HH′ + D product channel. Figure 2(b) shows the rotational state-resolved reaction cross sections of H + DH′ → HH′ + D reaction channel at $E_C = 0.5$ eV, the black squares are quantum-mechanical results with Boltzmann spin statistics reported by Chao *et al.*,[28] the red circles are experiment results, the blue stars are the TDWP results in this work. On the whole, these results agree well with each other, but from the details, it can be seen that our results for $j' = 1, 2, 4$ are closer to the experimental values than the ones obtained by Chao *et al.*

To shed light on the J dependence of the total reaction probabilities, we plot the reaction probabilities as a function of total angular momentum at eight collision energies in Fig. 3. The J-dependent partial wave contribution is weighted over a $(2J+1)$ factor to the ICS. It is well known that the J dependence of the ICS is an analog of the opacity function $p(b)$, where b is the collision parameter. Thus, different J dependence means different impact parameter dependence. All the opacity functions are smoothly varied and exhibit similar arch shapes. The curves follow the trend that increases with J, reaches the maximum and subsequently drops to zero when reaching the largest accessible value. Meanwhile, the curves extend to larger J values with increasing collision energy. It is also seen that for certain collision energy, large J partial waves are involved in the H + DH′ → HH′ + D channel, and in particular we can see from the vertical value that the bigger

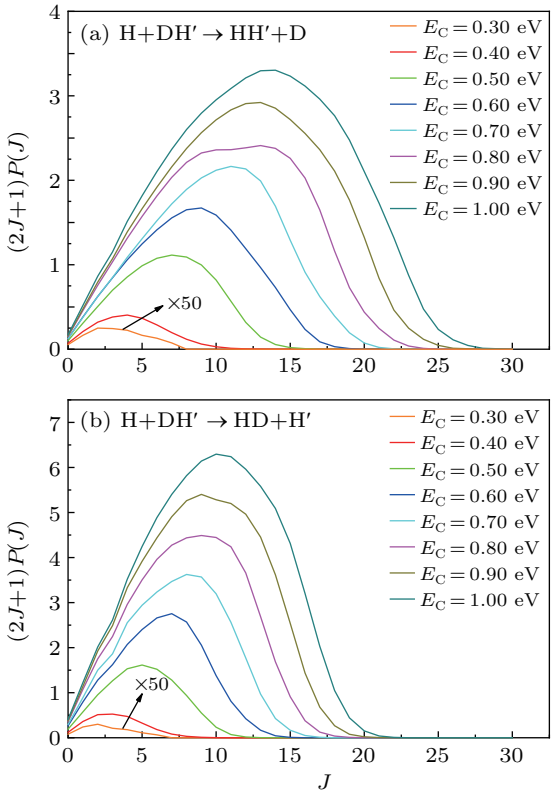


Fig. 3. $(2J+1)$ weighted opacity functions for (a) H + DH′ → HH′ + D and (b) H + DH′ → HD + H′ at different collision energies.

contributor to the H + DH′ → HD + H′ channel is the smaller J. According to the one-to-one correspondence between the impact parameter b and the angular momentum J, it is reasonable to consider that collisions with large impact parameters are in favor of the abstraction reaction, while those with small impact parameters lead to the exchange reaction.[43] Therefore, the direct abstraction mechanism is more dominant in H + DH′ → HH′ + D channel than H + DH′ → HD + H′.

3.2. Product distribution

Figure 4 shows the vibrational state-resolved reaction cross sections of the products HH′ and HD at the collision energy range of 0.15 eV–1.0 eV. As can be seen from Fig. 4, the products of both channels are mainly concentrated in the $v' = 0$ vibrational energy level. For HD product, because of lower vibrational frequency, the vibrational energy level of the product molecule can be reached is larger ($v' = 2$, and 1 for HD and H_2, respectively).

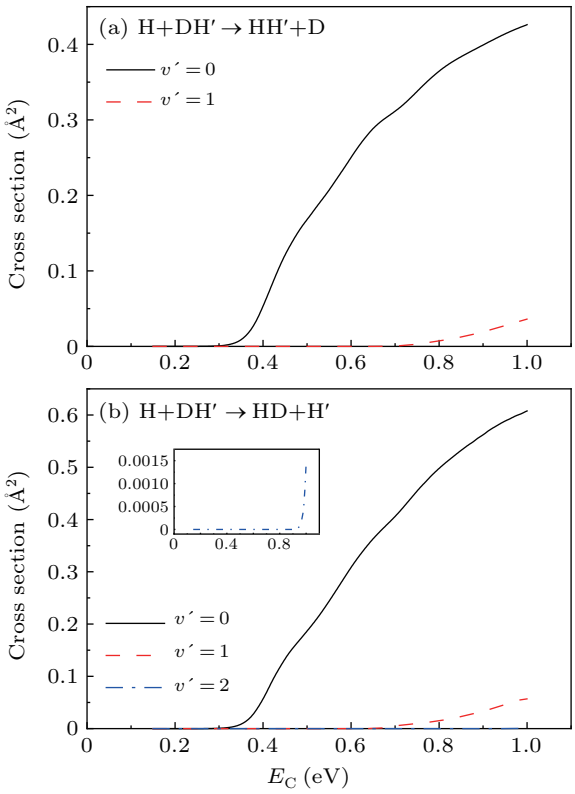


Fig. 4. Vibrational state-resolved reaction cross sections for (a) H + DH′ → HH′ + D and (b) H + DH′ → HD + H′ reactions.

The rotational state-resolved reaction cross sections of two product channels are also been calculated and shown in Fig. 5. There is a similar collision energy threshold (≈ 0.35 eV) for both reaction channels, and when the collision energy is greater than the threshold, the rotational quantum number inversion occurs in both reaction products. The difference is that the HD product channel can achieve a greater maximum rotational quantum number than the HH′ channel. Because the direct mechanism plays a major role in both reaction channels, and each atom in the system has a light mass, so the orbital angular momentum of the reactants can easily

be converted into the rotational angular momentum of the of the product molecules. Considering that the mass of atom D is higher than that of atom H, according to the rotational energy formula,

$$E_{\rm r} = \frac{\hbar^2}{2I} j'(j'+1), \tag{10}$$

the gap of rotational energy level of the HD molecule is small, and therefore, the maximum rotational energy level that the HD product molecule can achieve is larger.

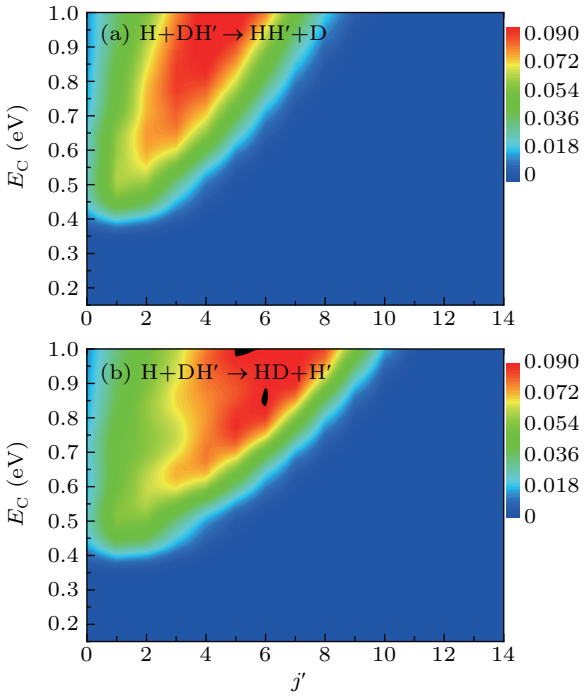


Fig. 5. Rotational state-resolved reaction cross sections for (a) $H + DH' \rightarrow HH' + D$ and (b) $H + DH' \rightarrow HD + H'$ reactions.

In order to more intuitively display the state distribution of product molecule, we plot the vib-rotational distribution at different collision energies for $H + DH' \rightarrow HH' + D$ and $H + DH' \rightarrow HD + H'$ channels in Figs. 6 and 7, respectively. It can be seen in these two figures that the vib-rotational distributions are like a half-cooked egg for both channels, the product's vibrational quantum number is essentially 0, and with the collision energy increasing, this half-cooked egg gets fatter and fatter, *i.e.*, the collision energy can promotes the rotational rather than vibrational excitation of the product molecules. In addition, it can also be seen from the difference between the Figs. 6 and 7 that the maximum rotational quantum number of HD achieved is greater than that of H_2. During the reactive encounter, total angular momentum is conserved

$$\boldsymbol{j}' + \boldsymbol{L}' = \boldsymbol{j} + \boldsymbol{L}, \tag{11}$$

here $\boldsymbol{L}'$ and $\boldsymbol{L}$ are the product and reagent orbital angular momenta. According to the impulse model[45] and

$$\boldsymbol{j}' = \boldsymbol{L}\sin^2\beta + \boldsymbol{j}\cos^2\beta + \boldsymbol{J}_1 m_B/m_{AB}, \tag{12}$$

for $A + BC \rightarrow AB + C$ reaction system,

$$\cos^2\beta = \frac{m_A m_C}{(m_A + m_B)(m_B + m_C)}, \tag{13}$$

$$\boldsymbol{J}_1 = \sqrt{\mu_{BC}E}(\boldsymbol{e}_{BA} \times \boldsymbol{e}_{BC}), \tag{14}$$

$\boldsymbol{e}_{BA}$ and $\boldsymbol{e}_{BC}$ are unit vectors with B pointing to A and B pointing to C, respectively; μ_{BC} is the reduced mass of BC molecule and E is the repulsive energy, the larger product atom will take more angular momentum away. Considering these two reaction channels in this work, $\boldsymbol{j} = 0$ and two $\boldsymbol{J}_1$s are the same. But for $H + DH' \rightarrow HH' + D$,

$$m_A = m_{\rm H},\ \ m_B = m_{\rm H'},\ \ m_C = m_{\rm D}, \tag{15}$$

$$\cos^2\beta \approx \frac{1}{3},\ \ \sin^2\beta \approx \frac{2}{3},\ \ \frac{m_B}{m_{AB}} \approx \frac{1}{2}, \tag{16}$$

while for $H + DH' \rightarrow HD + H'$,

$$m_A = m_{\rm H},\ \ m_B = m_{\rm D},\ \ m_C = m_{\rm H'}, \tag{17}$$

$$\cos^2\beta \approx \frac{1}{6},\ \ \sin^2\beta \approx \frac{5}{6},\ \ \frac{m_B}{m_{AB}} \approx \frac{2}{3}, \tag{18}$$

so the rotational quantum number $\boldsymbol{j}'$ of HD achieved is greater than that of HH'. In order to compare the energy level intervals quantitatively, we calculated the rotational energy levels of both the $HH'(v' = 0, j')$ and $HD(v' = 0, j')$ molecules by solving the radial Schrödinger equation of nuclear motion, and the results are shown in Table 2. From this table, it can be seen that HD has much smaller gaps of the rotational energy level.

Table 2. The vib-rotational energies (in units of $\rm cm^{-1}$) of the HH' and HD product molecules.

j'	$HH'(v'=0)$	$HD(v'=0)$
0	2179.93	1890.74
1	2298.44	1979.99
2	2534.36	2157.86
3	2885.57	2423.14
4	3348.92	2774.05
5	3920.41	3208.26
6	4595.24	3722.99
7	5367.94	4315.02
8	6232.56	4980.76
9	7182.75	5716.35
10	8211.88	6517.70
11	9313.22	7380.54
12	10479.96	8300.50

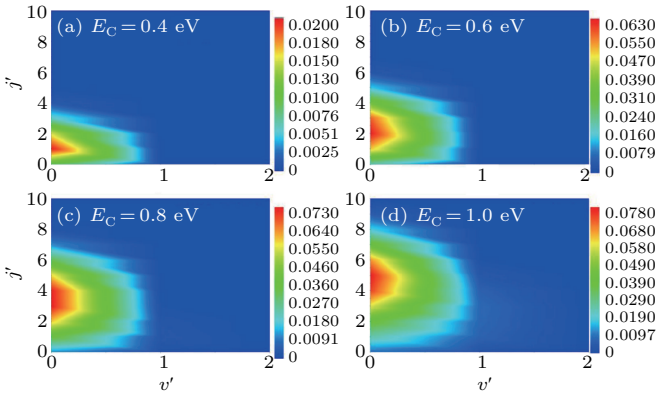


Fig. 6. Product vib-rotational state-resolved distributions for $H + DH' \rightarrow HH' + D$ reaction at four collision energies (a) $E_C = 0.4$ eV, (b) $E_C = 0.6$ eV, (c) $E_C = 0.8$ eV, and (d) $E_C = 1.0$ eV.

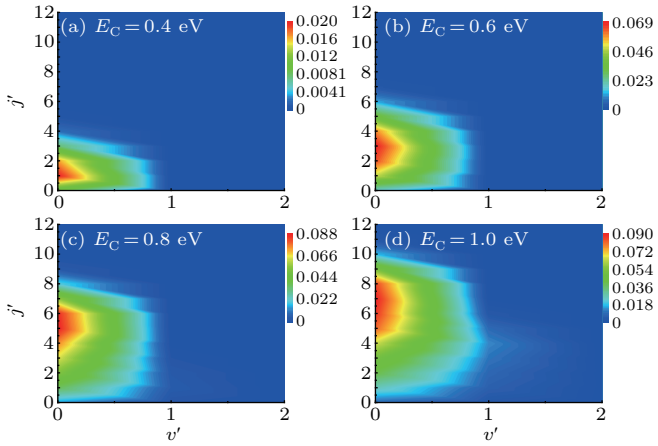


Fig. 7. The same as Fig. 6 but for $H + DH' \rightarrow HD + H'$ reaction.

3.3. Differential cross sections

Figures 8(a) and 8(b) display the total DCSs of $H + DH' \rightarrow HH' + D$ and $H + DH' \rightarrow HD + H'$ reaction channels at four collision energies, respectively. As can be seen in Figs. 8(a) and 8(b), the product of both channels are mainly backscattered, and with the collision energy increasing, the backward scattering is enhanced. Of course, there are some differences between these two channels. For $H + DH' \rightarrow HH' + D$ channel, the range of scattering angle is larger, and for $E_C = 1.0$ eV, a more obvious forward scattering phenomenon appears in $H + DH' \rightarrow HH' + D$ channel. These results are consistent with the usual rebound mechanism in a system with a collinear reaction path. Moreover, the center of mass of the reactant molecule DH' is closer to D, if the H atom approaches the reactant DH', it has a greater chance

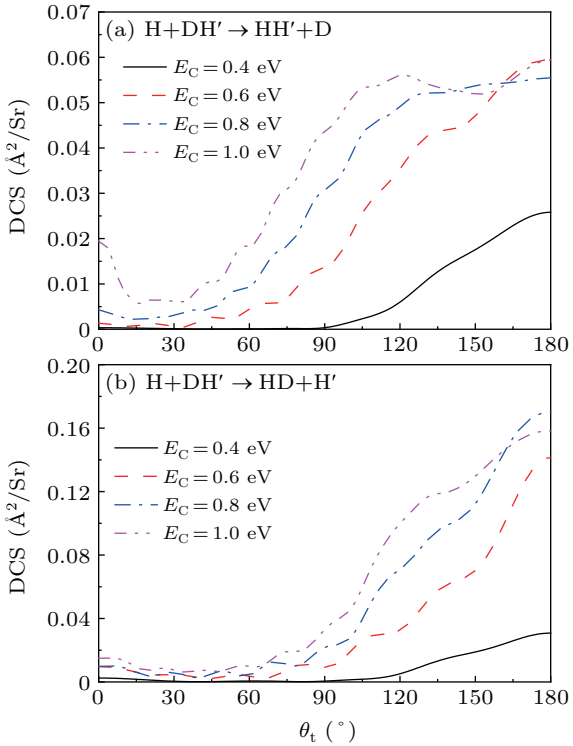


Fig. 8. Total DCSs for (a) $H + DH' \rightarrow HH' + D$ and (b) $H + DH' \rightarrow HD + H'$ reactions at four collision energies.

to get closer to D atom, and the reaction is controlled by the rebound mechanism, which leads to a larger scattering angle for HD product molecule than HH'. As the collision energy increases, larger number of partial waves are involved in the reaction[42] as shown in Fig. 3, which suggests that the contribution from the direct abstraction mechanism becomes larger, the scattering angle becomes smaller and the products start to scatter forward.

The individual state-to-state DCS reveals more angular structures than the total DCS. Figures 9 and 10 show the state-resolved DCSs of $H + DH' \rightarrow HH'(v' = 0, j') + D$ and $H + DH' \rightarrow HD(v' = 0, j') + H'$ reaction channels, respectively. It can be seen from the two figures that the products of the two channels present backward scattering distribution, especially for the small collision energy, the scattering angle is mainly concentrated at 180°. However, with the increase of the collision energy, the rotational quantum number of the product molecule becomes larger and larger, and the range of scattering angle gradually expands in the direction of decreasing.

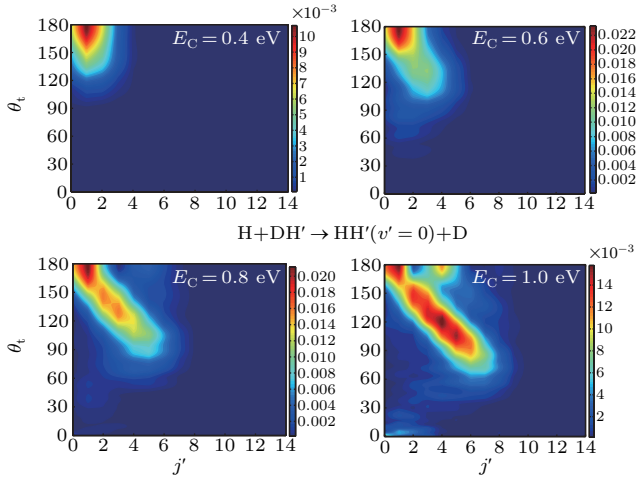


Fig. 9. The state-to-state DCS for $H + DH'(v = 0, j = 0) \rightarrow HH'(v' = 0, j') + D$ reaction at four collision energies.

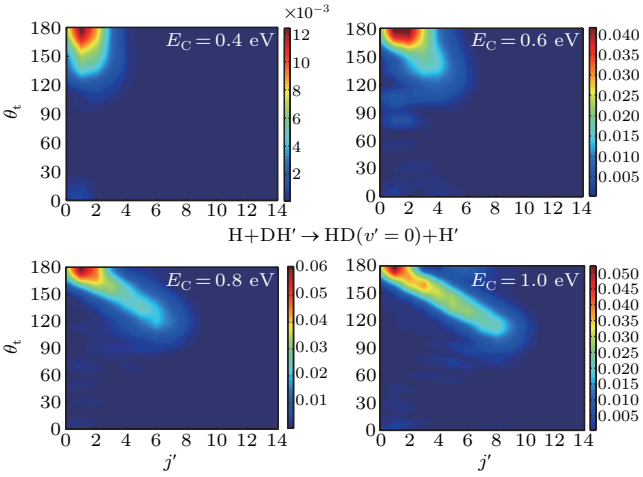


Fig. 10. The same as Fig. 9 but for $H + DH'(v = 0, j = 0) \rightarrow HD(v' = 0, j') + H'$ reaction at four collision energies.

In addition, there are some differences between the results of $H + DH' \rightarrow HH' + D$ and $H + DH' \rightarrow HD + H'$ chan-

nels. With the increase of the collision energy, the scattering angle of HH′ molecules decreases more rapidly. Moreover, at the collision energy of 1.0 eV, HH′ molecules with large rotational quantum number tend to have a more obvious sideway scattering distribution than that of HD, and the forward scattering HH′ molecules begin appear. This forward scattering is more obvious in the state-resolved DCSs of the product molecule with $v' = 1$, as shown in Fig. 11. It was further verified that the contribution of the direct abstraction mechanism in the HH′ product channel is greater than that in the HD channel at the higher collision energy. Moreover, HH′ molecules with $v' = 0$ and 1 both contribute to the forward scattering component.

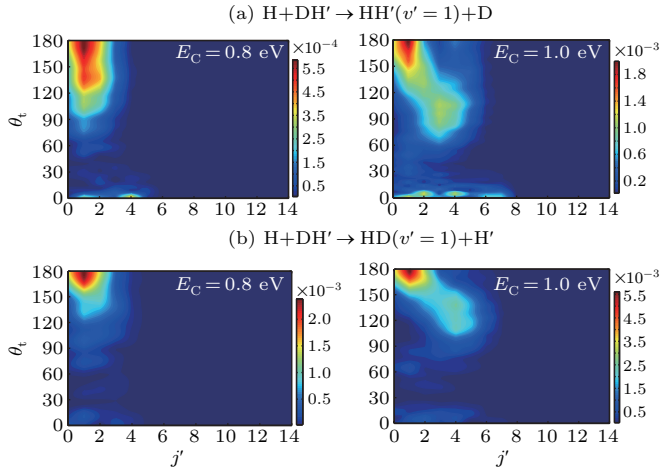


Fig. 11. The state-to-state DCSs for (a) $H + DH'(v = 0, j = 0) \rightarrow HH'(v' = 1, j') + D$ and (b) $H + DH'(v = 0, j = 0) \rightarrow HD(v' = 1, j') + H'$ reactions at the collision energy of $E_C = 0.8$ eV and 1.0 eV.

4. Summary

In this work, an efficient GPUs version of time-dependent wave-packet code has been used to calculate the differential cross section of $H + DH' \rightarrow HH' + D/HD + H'$ reactions on BKMP2 surface.

(i) There is a barrier in MEP, $H + DH' \rightarrow HH' + D/HD + H'$ reactions have threshold energy about 0.35 eV, which is lower than the barrier because of quantum tunnel.

(ii) By comparing with the earlier theoretical and experimental results of rotational state-resolved ICS of $H + DH' \rightarrow HH' + D$ reaction at the collision energy of 0.5 eV, it can be seen that our theoretical calculation results are closer to the experimental values for $j' = 1, 2, 4$, so, to some extent, our calculation accuracy is higher.

(iii) The opacity functions are smoothly varied and exhibit arch shapes, larger J partial waves are involved in the $H + DH' \rightarrow HH' + D$ channel and the bigger contributor to the $H + DH' \rightarrow HD + H'$ channel is the small J, according to the classical items, the direct abstraction mechanism is more dominant in $H + DH' \rightarrow HH' + D$ channel than $H + DH' \rightarrow HD + H'$.

(iv) Because of the smaller gap of rotational energy level of the HD molecule, the maximum rotational energy level of HD product molecule can achieve is larger than HH′.

(v) Although both reaction channels are predominantly backward scattered due to the rebound mechanism, the contribution of direct abstraction reaction mechanism will increase at the high collision energies, and the forward scattering distribution of HH′ is more obvious than that of HD.

All those show that the mass difference of isotopes can lead to a lot of differences in dynamics. Therefore, it is of great significance to study the isotopic effect on the dynamical properties.

Acknowledgment

The authors are very grateful to Prof. Han for providing the code.

References

[1] Wrede E, Schnieder L, Welge K H, Aoiz F J, Bañares L, Castillo J F, Haya B M and Herrero V J 1999 *J. Chem. Phys.* **110** 9971
[2] Harich S A, Dai D, Wang C C, Yang X, Chao S D and Skodje R T 2002 *Nature* **419** 281
[3] Harich S A, Dai D, Yang X, Chao S D and Skodje R T 2002 *J. Chem. Phys.* **116** 4769
[4] Ausfelder F, Pomerantz A E, Zare R N, Althorpe S C, Aoiz F J, Bañares L and Castillo J F 2004 *J. Chem. Phys.* **120** 3255
[5] Pomerantz A E, Ausfelder F, Zare R N, Marcos J C J, Althorpe S C, Rábanos V S, Aoiz F J, Bañares L and Castillo J F 2004 *J. Chem. Phys.* **121** 6587
[6] Koszinowski K, Goldberg N T, Pomerantz A E, Zare R N, Juanes-Marcos J C and Althorpe S C 2005 *J. Chem. Phys.* **123** 054306
[7] Wrede E and Schnieder L 1997 *J. Chem. Phys.* **107** 786
[8] Sun J C, Choi B H, Poe R T and Tang K T 1980 *Phys. Rev. Lett.* **44** 1211
[9] Haug K, Schwenke D W, Shima Y, Truhlar D G, Zhang J and Kouri D J 1986 *J. Phys. Chem.* **90** 6757
[10] Althorpe S C, Fernández Alonso F, Bean B D, Ayers J D, Pomerantz A E, Zare R N and Wrede E 2002 *Nature* **416** 67
[11] Mielke S L, Peterson K A, Schwenke D W, Garrett B C, Truhlar D G, Michael J V, Su M C and Sutherland J W 2003 *Phys. Rev. Lett.* **91** 063201
[12] Michael J V, Su M C and Sutherland J W 2004 *J. Phys. Chem. A* **108** 432
[13] Vaníček J, Miller W H, Castillo J F and Aoiz F J 2005 *J. Chem. Phys.* **123** 054108
[14] Juanes-Marcos J C and Althorpe S C 2005 *J. Chem. Phys.* **122** 204324
[15] Hankel M, Smith S C, Allan R J, Gray S K and Kurti G G B 2006 *J. Chem. Phys.* **125** 164303
[16] Chu T S, Han K L, Hankel M and Kurti G G B 2007 *J. Chem. Phys.* **126** 214303
[17] Chen M D, Han K L and Lou N Q 2002 *Chem. Phys. Lett.* **357** 483
[18] Truhlar D G and Horowitz C J 1978 *J. Chem. Phys.* **68** 2466
[19] Varandas A J C, Brown F B, Mead C A, Truhlar D G and Blais N C 1987 *J. Chem. Phys.* **86** 6258
[20] Boothroyd A I, Keogh W J, Martin P G and Peterson M R 1991 *J. Chem. Phys.* **95** 4343
[21] Boothroyd A I, Keogh W J, Martin P G and Peterson M R 1996 *J. Chem. Phys.* **104** 7139
[22] Mark Wu Y S, Kuppermann A and Anderson J 1999 *Phys. Chem. Chem. Phys.* **1** 929
[23] Aoiz F J, Bañares L and Herrero V J 1998 *J. Chem. Soc.* **94** 2483
[24] Aoiz F J, Bañares L and Herrero V J 2005 *Inter. Rev. Phys. Chem.* **24** 119
[25] Skouteris D, Castillo J F and Manolopoulos D E 2000 *Comp. Phys. Comm.* **133** 128
[26] Althorpe S C 2001 *J. Chem. Phys.* **114** 1601

[27] Kendrick B K 2000 *J. Chem. Phys.* **112** 5679
[28] Chao S D, Harich S A, Dai D X, Wang C C, Yang X and Skodje R T 2002 *J. Chem. Phys.* **117** 8341
[29] Schnieder L, Rahn K S, Wrede E and Welge K H 1997 *J. Chem. Phys.* **107** 6175
[30] Kendrick B K 2003 *J. Chem. Phys.* **118** 10502
[31] Dai D X, Wang C C, Harich S A, Wang X Y, Yang X M, Chao S D and Skodje R T 2003 *Science* **300** 1730
[32] Hochman Kowal S and Persky A 1997 *Chem. Phys.* **222** 29
[33] Zhang P Y and Han K L 2014 *J. Phys. Chem. A* **118** 8929
[34] Wei W, Gao S B, Sun Z P, Song Y Z and Meng Q T 2014 *Chin. Phys. B* **23** 073101
[35] Zhang Y C, Zhang Y B, Zhan L X, Zhang S L, Zhang D H and Zhang Z H J 1998 *Chin. Phys. Lett.* **15** 16
[36] Zhang J, Gao S B, Wu H and Meng Q T 2015 *J. Phys. Chem. A* **119** 8959
[37] Zhang J Y, Xu T, Ge Z W, Zhao J, Gao S B and Meng Q T 2020 *Chin. Phys. B* **29** 063101
[38] Zhang J, Gao S B, Wu H and Meng Q T 2015 *Chin. Phys. B* **24** 083104
[39] Zhang Y 2016 *Chin. Phys. B* **25** 123104
[40] Zhao J, Wu H, Sun H B and Wang L F 2018 *Chin. Phys. B* **27** 023102
[41] Xu T, Zhao J, Wang X L and T M Q 2019 *Chin. Phys. B* **28** 023102
[42] Wu H, Yao C X, He X H and Zhang P Y 2016 *J. Chem. Phys.* **144** 184301
[43] Wu H, Duan Z X, Yin S H and Zhao G J 2016 *J. Chem. Phys.* **145** 124305
[44] Fleck J A, Morris J R and Feit M D 1976 *Appl. Phys.* **10** 129
[45] Li R J, Han K L, Li F E, Lu R C, He G Z and Lou N Q 1994 *Chem. Phys. Lett.* **220** 281